Computer Physics Communications 182 (2011) 77–80

Contents lists available at ScienceDirect

Computer Physics Communications

www.elsevier.com/locate/cpc

Electronic properties of rhombohedral graphite

Jen-Hsien Wong [a], Bi-Ru Wu [b,*], Ming-Fa Lin [a,*]

[a] Department of Physics, National Cheng Kung University, Tainan, Taiwan
[b] Center for General Education, Chang Gung University, Taoyuan, Taiwan

ARTICLE INFO

Article history:
Received 27 February 2010
Received in revised form 10 July 2010
Accepted 14 July 2010
Available online 21 July 2010

Keywords:
Graphite
Energy bands
Electronic properties

ABSTRACT

Electronic properties of ABC-stacked graphite are studied by the first-principles method. There are linear and parabolic bands with strong anisotropic dispersions; both non-degenerate and degenerate bands are observed. The bandwidths of occupied π and σ bands are 8.41 eV and 16.65 eV, respectively. The low valence and conduction bands only have slight overlapping near the Fermi level, mainly owing to the interlayer atomic interactions. State degeneracy and energy dispersions are strongly affected by such interactions. The band-edge states, with the high density of states, are located near or at the high symmetry points. Some significant differences exist among ABC-, AB-, and AA-stacked graphites in electronic properties.

1. Introduction

Few-layer graphenes, such as monolayer, bilayer, and trilayer, have been produced by mechanical friction [1,2] and by thermal decomposition [3,4] in the past few years. A lot of researches have been performed for their unique two-dimensional physical properties, e.g., band structures [5,7–9], transport properties [10–12], optical spectra [6,13], and Coulomb excitations [13–16]. A monolayer graphene has two isotropic linear bands intersecting at the Fermi level, mainly owing to the hexagonal symmetry. It is a zero-gap two-dimensional semiconductor without free carriers. As for multilayer graphenes, the stacking configurations, such as AB- [5,6], AA-, and ABC-stacking [7], affects the electronic properties differently.

Bulk graphite consists of graphene layers periodically stacked along the $\hat{z}$ direction. It is one of the most important layered systems, and has been studied extensively both in experiments [17–21] and in theories [22–28]. There are four kinds of layered graphites: the rhombohedral graphite (the ABC-stacked graphite) [23,25], the Bernal graphite (the AB-stacked graphite) [26–28], the simple hexagonal graphite (the AA-stacked graphite) [27], and the turbostratic graphite (without the periodical stacking sequence) [24]. All of them are semimetallic because the interlayer atomic interactions induce the overlapping between the conduction and valence bands. Most natural graphite belongs to the AB-stacking sequence, and recently the AA- [19] and ABC-stacked [20,21] graphites have been produced in the lab. We study the electronic properties of the ABC-stacked graphite through the first-principles calculations. The low energy bands near the Fermi level are discussed in detail. To further understand the importance of stacking symmetry, a comparison with those of AB- and AA-stacked graphites is also presented.

2. First-principles calculation method

In this work, the electronic structure of the rhombohedral graphite is investigated by the density-functional theory (DFT) within the local-density approximation (LDA) [33–35]. The exchange-correlation energy is in the Ceperley–Alder form [36]. The ultrasoft pseudopotential is used for the carbon ions, as implemented in Vienna Ab-initio Simulation Package (VASP) [37]. The wave functions are expanded with the plane waves and the energy cutoff of 700 eV is carried out. A $30 \times 30 \times 30$ grid of k points in Monkhorst–Pack scheme is adopted in the first Brillouin zone sampling. All the atoms are relaxed until the Helmann–Feynman force is less than 0.01 eV/Å. The Fermi energy is determined by the use of the standard Gaussian smearing method with a broadening width of 0.01 eV.

A monolayer graphene has a honeycomb crystal structure. The rhombohedral graphite is built from the periodically ABC-stacked graphene layers along the $\hat{z}$ direction. Between adjacent layers, half of the atoms in the upper layer have the same xy coordinates with those in the lower one, while the other half fall on the center of the lower hexagon. A primitive unit cell includes six carbon atoms among three layers (Fig. 1(a)). To describe the rhombohedral lattice, three translation vectors are needed: $\vec{a}_1$ and $\vec{a}_2$ lie on the x–y plane with the magnitude of $\sqrt{3}b$, where b is the C–C bond length; $\vec{a}_3 = 3c\hat{z}$. $|\vec{a}_1| = |\vec{a}_2|$ and c is the interlayer distance. The points of high symmetry in the first Brillouin zone are shown in Fig. 1(b). The units of wave vector along $\hat{k}_x$ and $\hat{k}_z$ directions

* Corresponding authors.
E-mail addresses: brwu@mail.cgu.edu.tw (B.-R. Wu), mflin@mail.ncku.edu.tw (M.-F. Lin).

0010-4655/$ – see front matter
doi:10.1016/j.cpc.2010.07.030

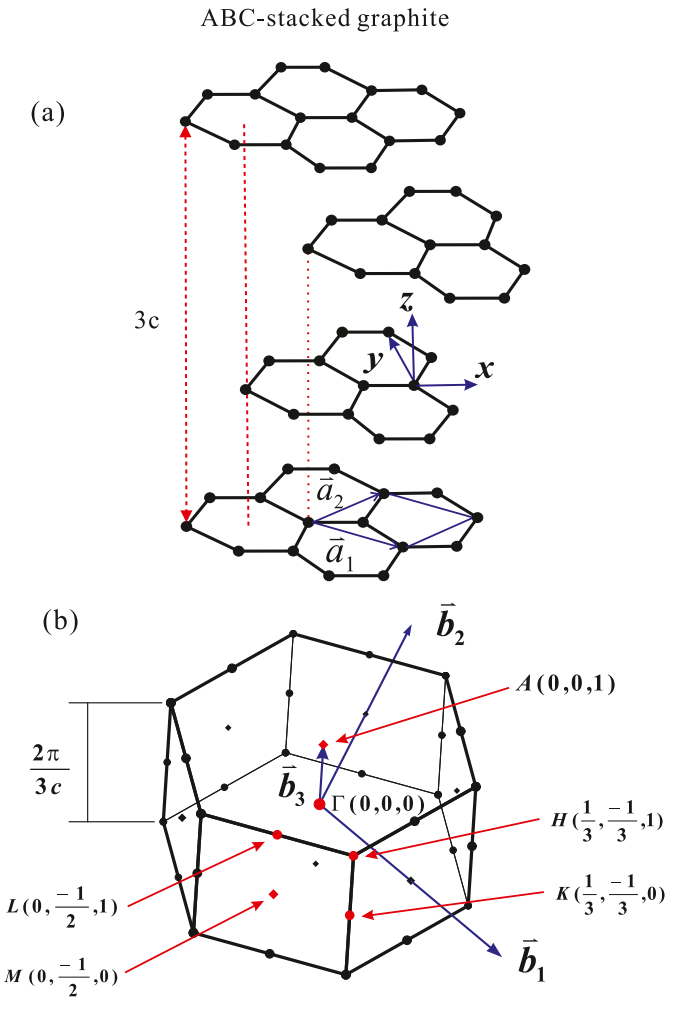

Fig. 1. (a) The rhombohedral graphite and (b) the first Brillouin zone. c is the interlayer distance.

are, respectively, $2\pi/\sqrt{3}b$ and $\pi/3c$. The calculated results of geometry optimization show that the bond length of rhombohedral graphite is 1.409 Å, which is close to those of AB- and AA-stacked graphites, 1.408 Å. The interlayer distances in ABC-, AB-, and AA-stacked graphites are 3.29 Å, 3.31 Å, and 3.58 Å, respectively. The total energy of ground state is −10.1617 eV/atom for the ABC-stacked graphite, −10.1618 eV/atom for the AB-stacked graphite, and −10.1523 eV/atom for the AA-stacked graphite. The former two graphites have the almost same value.

3. Electronic structures

Energy bands caused by the sp^2 and $2p_z$ orbitals are shown in Fig. 2. The occupied and unoccupied bands are not symmetric about the Fermi level $E_F = 0$. In the valence bands, there are 18σ subbands, and 9 subbands when spin degeneracy is not taken into account. There exists non-degenerate energy bands as well as double-, triple-, and six-fold degenerate ones. The highest and lowest energies in the σ bands are −3.07 eV and −19.72 eV at the Γ point, which defines the bandwidth of the σ bands, 16.65 eV. As for the π bands, 3 subbands exist near the Fermi level with the highest energy of ∼0 eV and the lowest of −8.41 eV, also giving the bandwidth. The calculated σ and π bandwidths can be verified by the photoelectron emission spectroscopy [29–31]. The π and π^* bands formed by the $2p_z$ orbitals only have slightly overlaps near $E_F = 0$; that is, the ABC-stacked graphite owns only a

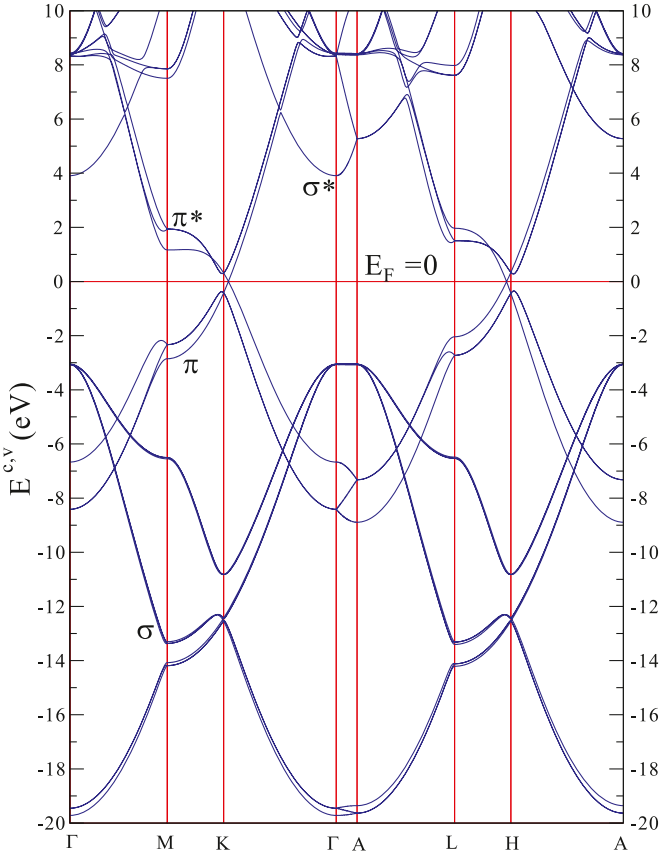

Fig. 2. The band structure of rhombohedral graphite along points of high symmetry.

few free carriers. The unoccupied σ^* bands start at 3.91 eV at the Γ point. All the energy bands show strong energy dispersions on the k_x–k_y plane, however they have weaker dependence on k_z. Each energy band owns a lot of band-edge states at or near the high symmetry points. The corresponding large density of states will have great influence on the essential physical properties. For example, the optical excitations from the π to the π^* bands near the M and L points are expected to exhibit pronounced peaks at absorption frequency ∼5–6 eV. Such peaks exist in the sp^2-related systems [32], e.g., carbon nanotubes, graphene nanoribbons, and carbon fullerenes. Two important differences in the low-energy bands can be seen when comparing this work to Refs. [23–25]. Fig. 2 illustrates that the linear crossing bands take place along $K \to \Gamma$ and $H \to A$. Nevertheless, gaps are opened in the figures of Refs. [23–25]. Moreover, the conduction and valence bands approach the Fermi level along $M \to K$, but the opposite is true in Ref. [23].

The low energy bands are drastically changed by the interlayer atomic interactions. A discussion for the $k_z = 0$ case is given first (the blue line in Fig. 3(a)). Three pairs of valence and conduction bands are located near $E_F = 0$; furthermore, the π and π^* bands are threefold degenerate at the K point. One of them (the first pair) are linear bands with no degeneracy and have an intersection (denoted as 00A) just above the Fermi level with wave vector of $[0.319, -0.319, 0]$. The other two pairs are double-degenerate parabolic bands. The maximum and minimum energies of parabolic bands are 0.29 eV and −0.38 eV along $M \to K$ with wave vectors of $[0.325, -0.338, 0]$ (00B) and $[0.322, -0.339, 0]$ (00C), respectively. When k_z grows from zero to one (Figs. 3(a)–(d)), the linear bands become parabolic ones with a subband gap, and the double degeneracy of the original parabolic bands is broken: One pair of the degeneracy-broken bands (the second one) becomes closer to the Fermi level, while the other pair (the third

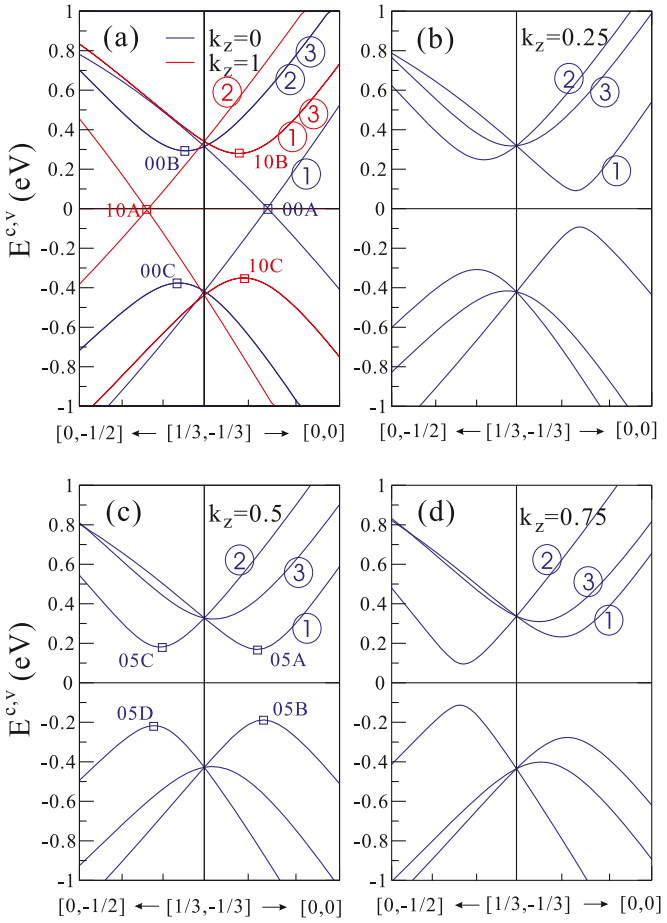

Fig. 3. The low energy bands for (a) $k_z = 0$ and $k_z = 1$, (b) $k_z = 0.25$, (c) $k_z = 0.5$; (d) $k_z = 0.75$ along $M \to K \to \Gamma$. The number inside an open circle represents the ith pair of valence and conduction bands. The wave vector between two ticks are 0.017 ($2\pi/\sqrt{3}b$). (For interpretation of the references to color in this figure, the reader is referred to the web version of this article.)

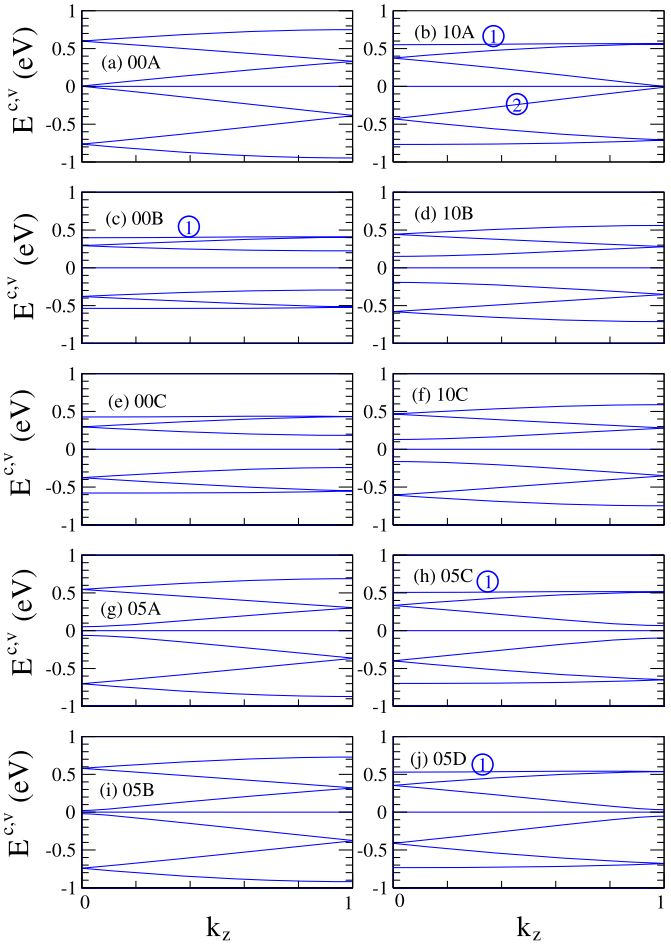

Fig. 4. The k_z-dependent energy dispersions near $E_F = 0$ for the special band-edge states.

one) departs from it along the $K \to M$ direction. However, the opposite is true for $K \to \Gamma$. The band-edge states in the first and second pairs (the third pair) move along the symmetry points, $\Gamma \to K \to M$ ($M \to K \to \Gamma$). At $k_z = 1$ (the red line in Fig. 3(a)) the first and third pairs combine and become parabolic bands with the original double degeneracy. The maximum and minimum energies of parabolic bands are 0.28 eV and -0.35 eV along $K \to \Gamma$ with wave vectors of $[0.326, -0.326, 1]$ (10B) and $[0.325, -0.325, 1]$ (10C), respectively. Moreover, the second pair changes into the linear bands with an intersection at $[0.308, -0.346, 1]$ (10A). In short, the low energy bands at $k_z = 0$ are virtually symmetric to those at $k_z = 1$ about the K point. The difference is that the intersection for $k_z = 1$ is right below the Fermi level (∼6 meV), while the one for $k_z = 0$ lies above (∼3 meV). The ABC-stacked graphite is a semimetal owing to the fact that a small amount of free carriers exists near the H (electrons) and the K (holes) points. It is worth noting that the four band-edge states (00B, 00C, 10B, 10C) makes certain distribution to the density of states. Their energies could be verified by scanning tunneling spectroscopy [38] directly, or by optical absorption spectroscopy indirectly [39].

The low energy bands are worthy of further investigation, and the k_z dependence owes to the interlayer atomic interactions. The special band-edge states in Figs. 3(a) and (c) are illustrated explicitly in Fig. 4. The energy bands, including linear and parabolic ones, are depicted along $\hat{k}_z$. The range of energy dispersions along $\hat{k}_z$, much weaker compared with those on k_x–k_y plane, is around 0.01–0.42 eV. The largest one (the second pair) takes place at 10A as shown in Fig. 4(b), while Figs. 4(b), (c), (h), and (j) all show a range of around 0.01 eV, which corresponds to the first pair. In terms of states degeneracy, it might happen at $k_z = 0$ and $k_z = 1$. The non-degenerate bands at $k_z = 0$ become double-degenerate ones at $k_z = 1$, and vice versa. No gap is seen at 00A and 10A, as shown in Figs. 4(a) and (b). The rest all exhibit a subband gap.

There are certain important differences among three kinds of graphites, as shown in Fig. 5 at $k_z = 0$. For ABC-stacked graphite, three pairs of valence (π) and conduction (π^*) bands are located near the K point; two of them are degenerate parabolic bands, and the other is non-degenerate linear ones. Two pairs of non-degenerate parabolic bands exist in AB-stacked graphite. One of them has two intersections below the Fermi level with one at the K point, and the other near it. As for AA-stacked graphite, there is only one pair of non-degenerate linear bands intersecting at the K point above $E_F = 0$. The three systems have the band-edge states of different positions. For example, at $k_z = 0$, the band-edge states of AA-stacked graphite are located at the K point, while those of AB- and ABC-stacked ones lie near it. AA-stacked graphite has the largest band overlap, while ABC-stacked graphite has the smallest one, which means that it has the least number of free carriers due to the complex stacking configuration. The main differences among three systems are caused by the stacking symmetry and the interlayer atomic interactions. Since AA-stacked graphite has the highest symmetric configuration, it shows the strongest energy dispersions along $\hat{k}_z$, the largest overlapping of energy bands, and the greatest free carrier density. Nevertheless, the ABC-stacked graphite exhibits the opposite behavior.

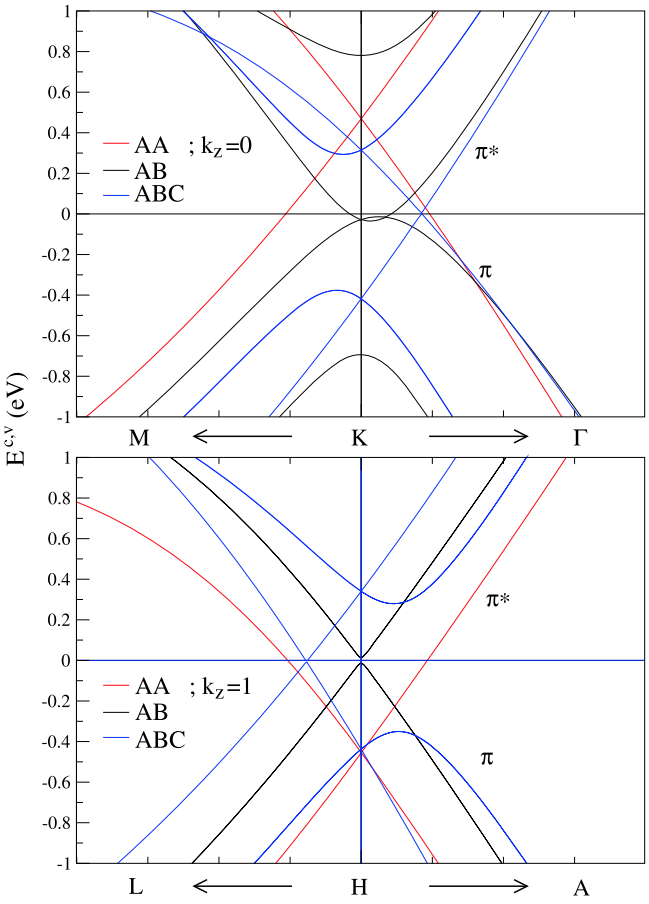

Fig. 5. The π and π^* energy bands for ABC-, AB-, AA-stacked graphites. The wave vector between two ticks are 0.029 ($2\pi/\sqrt{3}b$).

4. Concluding remarks

The ABC-stacked graphite owns linear and parabolic energy bands with strong anisotropy. Energy bands may be non-degenerate as well as double, triple, and six-fold. Each band has many band-edge states contributing to the high density of states. Such states are located near or at the high symmetry points. The bandwidths of occupied π and σ bands are 8.41 eV and 16.65 eV, respectively. For the low energy bands, there exist double-degenerate parabolic bands and non-degenerate linear bands with one intersection above the Fermi level near the K point, and the other below it near the H point. The weak overlapping between the π and π^* bands results in the semimetallic properties. When viewed along $\hat{k}_z$, the linear bands become parabolic ones with a subband gap, and the double degeneracy of the original parabolic bands is broken. At the linear intersections, as well as the local maxima and minima, the range of energy dispersion is ~0.01–0.42 eV along $\hat{k}_z$. The k_z dependence is much weaker than those on the k_x–k_y plane. Among these three systems, AA-stacked graphite has the largest band overlap, while ABC-stacked graphite has the smallest. As a consequence, ABC-stacked graphite exhibits the weakest energy dispersion, which is the results of stacking symmetry. The predicted electronic properties could be verified by the experimental measurements on scanning tunneling currents, photoelectron emission spectra, and optical absorption spectra.

Acknowledgements

This work partially supported by the NSC and NCTS of Taiwan, under the Grant Nos. NSC 98-2112-M-006-013-MY4, and NSC 97-2112-M182-003.

References

[1] K.S. Novoselov, A.K. Geim, S.V. Morozov, D. Jiang, Y. Zhang, S.V. Dubonos, I.V. Grigorieva, A.A. Firsov, Science 306 (2004) 666.
[2] K.S. Novoselov, A.K. Geim, S.V. Morozov, D. Jiang, M.I. Katsnelson, I.V. Grigorieva, S.V. Dubonos, A.A. Firsov, Nature London 438 (2005) 197.
[3] C. Berger, Z.M. Song, T.B. Li, X.B. Li, A.Y. Ogbazghi, R. Feng, Z.T. Dai, A.N. Marchenkov, E.H. Conrad, P.N. First, W.A. de Heer, J. Phys. Chem. B 108 (2004) 19912.
[4] C. Berger, Z. Song, X. Li, X. Wu, N. Brown, C. Naud, D. Mayou, T. Li, J. Hass, A.N. Marchenkov, E.H. Conrad, P.N. First, W.A. de Heer, Science 312 (2006) 1191.
[5] C.L. Lu, C.P. Chang, Y.C. Huang, R.B. Chen, M.L. Lin, Phys. Rev. B 73 (2006) 144427.
[6] C.L. Lu, C.P. Chang, Y.C. Huang, J.M. Lu, C.C. Hwang, M.F. Lin, J. Phys.: Condens. Matter 18 (2006) 5849.
[7] Y.H. Lai, J.H. Ho, C.P. Chang, M.F. Lin, Phys. Rev. B 77 (2008) 085426.
[8] M. Aoki, H. Amawasi, Solid State Commun. 142 (2007) 123.
[9] S. Latil, L. Henrard, Phys. Rev. Lett. 97 (2006) 036803.
[10] J. Nilsson, A.H. Castro Neto, F. Guinea, N.M.R. Peres, Phys. Rev. Lett. 97 (2006) 266801.
[11] Y. Zhang, Y.W. Tan, H.L. Stormer, P. Kim, Nature London 438 (2005) 201.
[12] K.S. Novoselov, E. McCann, S.V. Morozov, V.I. Fal'ko, M.I. Katsnelson, U. Zeitler, D. Jiang, F. Schedin, A.K. Geim, Nat. Phys. 2 (2006) 177.
[13] Y.H. Ho, Y.H. Chiu, D.H. Lin, C.P. Chang, M.F. Lin, Acs Nano 4 (2010) 1465.
[14] X.-F. Wang, T. Chakraborty, Phys. Rev. B 75 (2007) 041404(R).
[15] N.M.R. Peres, F. Guinea, A.H. Castro Neto, Phys. Rev. B 72 (2005) 174406.
[16] J.H. Ho, C.L. Lu, C.C. Hwang, C.P. Chang, M.F. Lin, Phys. Rev. B 74 (2006) 085406.
[17] T. Matsui, H. Kambara, Y. Niimi, K. Tagami, M. Tsukada, H. Fukuyama, Phys. Rev. Lett. 94 (2005) 226403.
[18] W.W. Toy, M.S. Dresselhaus, G. Dresselhaus, Phys. Rev. B 15 (1977) 4077.
[19] J.K. Lee, S.C. Lee, J.P. Ahn, S.C. Kim, J.I.B. Wilson, P. John, J. Chem. Phys. 129 (2008) 234709.
[20] H.A. Wilhelm, B. Croset, G. Medjahdi, Carbon 45 (2007) 2356.
[21] W. Kohs, H.J. Santner, F. Hofer, H. Schröttner, J. Doninger, I. Barsukov, H. Buqa, J.H. Albering, K.-C. Möller, J.O. Besenhard, M. Winter, J. Power Sources 119 (2003) 528.
[22] P.R. Wallace, Phys. Rev. 71 (1947) 622.
[23] J.C. Charlier, X. Gonze, J.P. Michenaud, Carbon 32 (1994) 289.
[24] J.C. Charlier, J.P. Michenaud, P. Lambin, Phys. Rev. B 46 (1992) 4540.
[25] J. Furthmüller, J. Fafner, G. Kresse, Phys. Rev. B 50 (1994) 15606.
[26] J.C. Charlier, J.P. Michenaud, X. Gonze, Phys. Rev. B 46 (1992) 4531.
[27] J.C. Charlier, J.P. Michenaud, X. Gonze, J.P. Vigneron, Phys. Rev. B 44 (1991) 13237.
[28] G. Dresselhaus, Phys. Rev. B 10 (1974) 3602.
[29] T. Ohta, A. Bostwick, J.L. McChesney, T. Seyller, K. Horn, E. Rotenberg, Phys. Rev. Lett. 98 (2007) 206802.
[30] S. Xu, J. Cao, C.C. Miller, D.A. Mantell, R.J.D. Miller, Y. Gao, Phys. Rev. Lett. 76 (1996) 483.
[31] B. Reihl, J.K. Gimzewski, J.M. Nicholls, E. Tosatti, Phys. Rev. B 33 (1986) 5770.
[32] M.F. Lin, Kenneth, W.-K. Shung, Phys. Rev. B 50 (1994) 17744.
[33] G. Kresse, J. Hafner, Phys. Rev. B 47 (1993) R558.
[34] G. Kresse, J. Hafner, J. Phys.: Condens. Matter 6 (1994) 8245.
[35] G. Kresse, J. Furthmüller, Comput. Mater. Sci. 6 (1996) 15.
[36] D.M. Ceperley, B.J. Alder, Phys. Rev. Lett. 45 (1980) 566.
[37] G. Kresse, J. Hafner, Phys. Rev. B 47 (1993) 558;
G. Kresse, J. Furthmüller, Phys. Rev. B 54 (1996) 11169.
[38] B. Premlal, M. Cranney, F. Vonau, D. Aubel, D. Casterman, M.M. De Souza, L. Simon, Appl. Phys. Lett. 94 (2009) 263115.
[39] S.H. Jeong, K.K. Kim, S.J. Jeong, K.H. An, S.H. Lee, Y.H. Lee, Synth. Met. 157 (2007) 570.